A STUDY OF MWPC WITH CHEVRON CATHODE PAD READOUT

J. Barrette, Y. Dai, K. Filimonov, S.K. Mark, Y.J. Qi, M. Rosati, N. Starinski, M. Wang* and B.Zhang*
Foster Radiation Laboratory, McGill University, Montreal, Canada

B. Yu
Brookhaven National Laboratory, Upton, NY 11973, USA

Dec. 8,1995

Abstract

An investigation of MWPCs with interpolating chevron shaped cathode pad readout has been carried out as part of the R&D for the particle tracking system of the PHENIX detector at RHIC. Two prototype chambers were designed and constructed. Their response to minimum ionizing particles was tested with secondary beams from the Alternating Gradient Synchrotron (AGS) at Brookhaven National Laboratory. Results on resolution, differential non-linearity and overall performance for different chevron patterns and cell geometries are presented.

*Permanent address: Institute of high Energy Physics, Academica Sinica, Beijing, China

1. Introduction

The tracking system of the PHENIX detector [1] at RHIC includes three cathode pad chambers which will perform measurements of non-projective three dimensional spatial points to be used mainly to help in pattern recognition. The design of the PHENIX tracking system imposes several constraints on the pad chambers. These detectors should have good spatial resolution in order to provide efficient track reconstruction and good momentum resolution and furthermore the effective thickness of each detector should correspond to ≈0.5% of a radiation length to minimize photon conversion. This represents a challenge for the construction of the chambers, particularly because of their large size. It has been shown that interpolating pad chambers can be used to obtain position information much finer than the readout spacing thus reducing the number of necessary readout channels, an important factor in the construction and cost of such detector.

Pad detectors are multiwire proportional chambers (MWPC), in which one or both cathode planes are divided into sensitive pads that are used to determine the position of particles traversing the detector. Charged particles passing through the active gas volume produce ionization along their trajectories. Electrons drift to the nearest anode wire where an avalanche occurs. The resulting ion cloud induces, by capacitive coupling, a charge distribution on the cathode pads close to the avalanche location. There are several schemes for the determination of the position of the avalanche. They can be roughly divided into three categories: resistive charge division [2, 3, 4, 5, 6], capacitive charge division [7, 8] and geometrical charge division [9, 10, 11, 12, 13, 14, 15]. In the geometric charge division method, pads of a specific geometric shape are used to sample the charge induced on the cathode, and the relative value of the induced charges on the pads determines the avalanche location.

This paper describes the design, construction and testing of two prototype pad chambers developed for PHENIX. These detectors used geometrical interpolation with pads of chevron geometry. The detector design and construction are described in the next section. The results of beam tests and detector performances are presented in Section 3.

2. Detector Construction

A chevron pad detector has chevron shaped pads as a cathode. The induced charge is shared by at least two neighboring chevron pads so that position of the avalanche is, to first order, proportional to the amount of charge deposited on each pad. Such design allows a significantly larger readout node spacing than that using rectangular pads and thus results in a reduced number of readout channels. Several different types of chevrons have been investigated [16, 17]. The types of chevron geometry tested here are sketched in Fig. 1. The chevron geometry is characterized by the chevron width w_a, the node spacing l_a, and the length of the chevron pattern defined to be $f_x l_a$, where f_x is a form factor that determines the amount of overlap h_a between the chevrons. All tested patterns are of the class of "single centered chevron". Centered chevrons are configured so that the anode wire runs over the chevron apex. They were selected because the measured charge ratios, and thus position measurement, is to first order insensitive to a small lateral displacement of the anode wire. "Single" refers to the fact that there is only one chevron period in one pad width. Patterns with multiple chevrons are expected to have better intrinsic differential non-linearity [17]. However, the present design has very large ratios of the pad length to the pad width resulting in very small angles for the chevron. Multiple chevron would imply in even sharper angles that would impose very severe requirements on the cathode fabrication. Even small imperfections in the etching of the pads would result in large systematic errors in the position determination. In this work, two types of such chevron have been investigated. The first type (Fig. 1(a)) is the "normal"chevron with pointed tips and tails. The second type (Fig. 1(b,c)) is the "squared"chevron which has tips truncated. Such a design is easier to manufacture and it considerably reduces the effect of variations in the width of the isolated traces on the effective length of the pads. In the tested cathodes, the tips were truncated to a minimum width $\delta = 250$ μm.

The main dimensions of the tested prototypes are given in Table 1. The PC94 prototype is designed to investigate the chamber performance as a function of f_x. It has a "standard"square cell geometry with an anode to cathode spacing of 2 mm and an anode to anode wire spacing of 4 mm corresponding to a 4 mm $\times$ 4 mm cell size. In this prototype, the chevron width is 3 mm and the pad length, l_a, has a fixed value of 220 mm. Rows of chevrons are separated by a guard strip of width 0.50 mm and the width of the isolated traces is set to 0.250 mm. PC94 is divided into two sections. One section has three patterns of standard single centered chevrons (Fig. 1a) with f_x values of 1.15, 1.21, ad 1.25 corresponding to a calculated overlap, h_a, of -9.2, 1.8, and 9.2 mm respectively (Negative sign means no overlap). The second section has three patterns of squared chevrons (Fig. 1b) with f_x values of 1.35, 1.40, 1.45 corresponding to h_a of 2.8, 11, and 19.2 mm. The active area of the detector is 144 cm by 8 cm, with a total of 140 readout channels. In order to check for reproducibility of the results, each of the six tested patterns covered a minimum of three adjacent pad rows.

In the PC95 prototype, the chevron patterns have not only squared tips but also squared tails with $\delta' = 125$ μm as shown in Fig. 1c. This prototype is divided in three sections with different cell sizes and pad lengths (see Table 1). The geometry of these sections was selected to represent the expected geometry of the three pad chambers of the PHENIX detector. The ratio of the pad width to the cell width was decreased as compare to PC94 in order to reduce charge sharing between neighboring cells (see below). The larger width of the cells results also in a smaller fraction of particles crossing two adjacent cells and thus in a lower effective occupancy of the detector. Each sector had three anode wires and a active length corresponding to five chevrons.

The mechanical structure of PC95 is shown on Fig. 2. PC94 has a similar structure.

The pad cathode planes are two-layer copper clad FR4 printed circuit boards with rows of pads and guard strips etched on one side and readout traces on the other. The two sides are connected by plated through holes. The second cathode planes are made of 25 μm thick aluminized mylar foils. In order to maintain a constant anode-cathode separation, the printed circuit board and mylar planes are reinforced by gluing with 22.86 mm and 6.35 mm thick sheets of low mass HEXCELL honeycomb and backed with 250 μm thick FR4 skins. Such technique provides structural rigidity and the required flatness with small amount of material. The cathode boards and electronics are mounted on a machined FR4 frame. The anode wires are made of gold plated tungsten rhenium wires of 25 μm diameter placed half way in between the cathode planes. The field wires made of beryllium-copper wires of 125 μm are placed in between the sense wires. The anode wires were set at positive potential while the field wires and cathode planes were grounded. The gas used in the detector was 50% argon and 50% ethane.

Each pad has its own electronic readout. The readout leads are connected to electronic boards installed at the edge of the detector on the FR4 frame. The electronics chain for the prototype chamber consists of a charge sensitive preamplifier, a shaping amplifier, and a digital converter (Fig. 3.). The preamplifier used is a three channel charge sensing hybrid type BNL-IO-454-4. It is a low noise, high performance inverting preamplifier with a feedback loop through a capacitor. The output of a preamplifier is processed by a bipolar shaping amplifier with a 200 ns shaping time. The output of the shaping amplifier is digitized by a 11 bit LeCroy 2249W ADC using a 200 ns wide gate. The nominal operating voltage during the test was 1600 V for PC94 and 1825 V, 2000 V, and 2250 V for the three sections of PC95, respectively.

3. Detector Performance

The prototypes were tested in the B2 beamline of the Alternating Gradient Synchrotron (AGS) at BNL using a secondary beam of e^-'s and π^-'s of various momenta between 0.5 and 10 GeV/c. The beamline was instrumented with three beam defining scintillation counters ($S1, S2, S3$) and a tracking chamber (Fig. 4.). The tracking chamber is a high resolution two-dimensional gas proportional detector [18]. It was used to get accurate coordinates of the beam particle. Its resolution in the direction of the anode wires of the prototype is less than 300 μm. The prototype detector was mounted on a precision moving stage allowing to locate the pad detector with respect to the tracking chamber. The data acquisition system was controlled by a Macintosh connected to the VME crate. Data from both detectors were written to 8-mm tape. The pad detectors were scanned over several chevron lengths along the wire direction and measured position then compared with true position given by the tracking chamber.

3.1. Position linearity

Pad chambers using the center of gravity method for impact reconstruction are known to have large non-linear systematic effects [16, 17, 19, 20]. The degree of non-linearity, however, depends on pad geometry and can be reduced to a tolerable level by proper design of the pad. To first order the reconstructed position of the avalanche in a MWPC with chevron cathode pad readout can be calculated as:

$$x_{rec} = \frac{Q_{A,B}}{Q_A + Q_B} \cdot l'_a + X^c_{A,B}, \tag{1}$$

where Q_A, Q_B are the charges induced on two neighboring chevrons, l'_a is the effective node spacing, and $Q_{A,B}$ and $X^c_{A,B}$ are the induced charge and the centroid coordinate of pad A or B, respectively. The value of l'_a is adjusted so that x_{rec} matches at the transition between successive chevrons.

The difference between the reconstructed position x_{rec} and the coordinate x_{true} given by the tracking chamber is presented in Fig. 5(a) as a function of the avalanche location for the normal chevron pattern in PC94 with f_x=1.25. This difference shows a strong and well defined dependence on the position with a pattern having a frequency corresponding to the node spacing. Each row with the same f_x value gives consistent non-linearity pattern, demonstrating that the observed non-linearity is mainly related to the pad geometry. A very similar behavior is observed for the two other tested values of f_x. The distribution of the residuals has a resolution σ=6 mm (Fig. 5b).

The measured differential non-linearity depends on the functional form used to calculate the measured avalanche position. It is possible to partly correct for non-linearity using relatively fast and simple algorithms which could be considered for use on-line. Computer simulations have shown [1] that effective linearization can be obtained using a quadratic correction of the form:

$$x_{cor} = x_{rec} + \alpha \cdot \frac{Q_A \cdot Q_B}{Q_A + Q_B} + \beta, \tag{2}$$

where α, β are parameters to be adjusted for a given chevron geometry. The results of this correction are shown in Fig. 5(c,d). It brings the global position resolution to σ=2.9 mm.

This can be compared to the average intrinsic position resolution due to other sources than non-linearity effects. This resolution was obtained by centering bin by bin the distribution of residuals shown in Fig. 5(a). The results are shown in Figs 5(e) and 5(f). The intrinsic position resolution of the detector assuming 'perfect' linear response is σ=2.4 mm.

In general, a smaller non-linearity has been observed for the pads with chopped off tips (squared chevrons). The (uncorrected) residual distribution for such chevron geometry with f_x = 1.35 is shown in Figs. 6(a) and 6(b). It yields better global accuracy (σ=4.3 mm) and linear response than for chevrons with pointed tips. However, due to asymmetry in $\frac{Q_A \cdot Q_B}{Q_A + Q_B}$ distribution the quadratic correction is not as effective, improving the global position resolution only to 3.5 mm (Figs. 6(c) and 6(d)).

Another way to correct for non-linearity is to compare the reconstructed coordinate with some calibration curve. The residual $x_{rec} - x_{true}$ can be fitted as a function of reconstructed position by a simple function, for instance assuming a linear dependence:

$$x_{cor}^{lin} = \alpha_1 \cdot \mid (x_{rec} + X^c) \mid + \beta_1, \tag{3}$$

or a parabolic function:

$$x_{cor}^{par} = \alpha_2 \cdot (x_{rec} + X^c)^2 + \beta_2, \tag{4}$$

where X^c is the centroid coordinate equivalent to $X_{A,B}^c$ in eq. 1. The parameters $\alpha_1, \beta_1, \alpha_2, \beta_2$ are assumed to be the same for all pads with the same geometry. The results of this procedure for squared chevron pattern with $f_x = 1.35$ are presented in Fig. 7. Both functions work very well, almost completely linearizing the response of the chamber and improving global resolution to σ=2.4 mm. This should be compared to the 'perfect' off-line correction σ=2.3 mm (Fig. 6(f)). For normal chevron pattern this method works as well as the one using quadratic correction.

3.2. Position resolution

The intrinsic resolution for the various tested geometries was investigated using the technique described above, i.e. by correcting the distribution of measured position bin by bin. The measured resolution does not take into account the accuracy of the tracking detector used to determine the "true" position of the tracks. The resolution of the tracking detector has been measured to be ≈100 μm [18] and its contribution to the measured position resolution is considered to be negligible. The results for PC94 averaged over all wires with the same f_x are summarized in Table 2. Both chevron types in PC94 give comparable results. The resolution is consistently between 1 to 1.5% of the node spacing.

As mentioned above, the form factor f_x defines the amount of overlap of the chevron tips and tails. Generally, one has to avoid using large values of f_x as it might require involving three pads in single track reconstruction, thus complicating pattern recognition at high multiplicities. For chevrons with too small f_x there is a region where charge is induced only on one pad and the centroid method does not work. This explains the worst resolution obtained for normal chevron with $f_x = 1.15$ for which h_a= −9.2 mm. This explains also that the pattern with $f_x = 1.21$, which computer simulations predicted to give the best results, has a worse resolution than $f_x = 1.25$. It is believed to be caused primarily by the quality of etching of the cathode board. Very fine tips and tails of pointed chevron were etched away thus increasing the effective gap between the apices of the chevrons. The measurements of actual cathode showed that in average the real overlaps for normal chevrons are reduced by ********≈ 5 mm ****** relative to those in the original drawing. For squared chevrons this effect is negligible.

For squared chevron patterns, the position resolution degrades with larger f_x-value. This effect can be explained partly by the fact that larger f_x value leads to smaller angles for the chevrons and, as a consequence, to larger sensitivity to error in the measured charges. One can thus conclude that for chevron patterns with very large aspect ratios like those tested here the optimum design corresponds, in general, to one with no or very small value of the overlap h_a.

The resolutions obtained with PC95 are 1.44 mm, 1.41 mm, and 1.71 mm for Sect.1, Sect.2 and Sect.3, respectively. This resolution is comparable to that observed with PC94 and corresponds to less than 1.5% of the node spacing.

The various contributions to the resolution have been studied by comparing resolutions at different values of deposited charge. Typical distributions of the total charge induced on the chevron cathodes during the beam test are presented in Fig. 8(a) and 8(b). The resolution dependence on the total charge is given in Fig. 8(c) for the chevron of normal type with $f_x = 1.25$ and the chevron of squared type with $f_x = 1.35$, and in Fig. 8(d) for the three sections of PC95. The data are well described by a relation of the form:

$$\sigma = \sqrt{\sigma_1^2 + \frac{\sigma_2^2}{Q_{total}^2}}. \tag{5}$$

The parameter σ_1 represents the resolution limit reached for very large signal. It is equal to about 1.5 mm for PC94 and varies between 1.1 and 1.3 mm for the three sections of PC95. This limit is possibly determined by lateral variation in the location of avalanche and by the quality of the etching of the cathode board. The parameter σ_2 is mainly determined by the electronic noise. During the beam tests the noise contribution in each electronic channel (corresponding to an individual chevron) had an average width σ_{noise}=3 ADC channels for PC94 while it was typically 2, 5, and 7 ADC channels for the three sections of PC95. One ADC channel corresponds to an input signal of roughly 1000 electrons. The observed increase in the electronic noise of the different sections of PC95 is consistent with the relative increase of the capacitance of the chevron. In the tested conditions, the electronic noise contributes roughly half of the observed total position resolution.

3.3: Charge Sharing Across the Wire Direction

Because of the relatively large spread of the induced charge on the cathode plane, some charge will be induced on the pads under the two neighboring wires. It is important to minimize this charge sharing since it will add to the effective occupancy of the detector. Furthermore, even a small sharing can degrade significantly the position measurement for particles hitting simultaneously two adjacent sets of pads.

We have studied the charge sharing using both beam particles and, for PC95, 5.9 KeV X-rays produced by a ^{55}Fe source. The X-rays from the ^{55}Fe source were collimated to a 0.8 mm circular beam spot centered on a wire. The beam particles were uniformly distributed across the chevron. The measured charge sharing as a fraction of the charge measured on the center row is given in Table 3 for the various cell dimensions studied. The numbers given correspond to the mean of the values measured on the two adjacent pad rows. Some difference is observed between the two adjacent rows that can be explained by a small displacement of the anode wire where the avalanche occured. In spite of the presence of ground strips, which increase the separation of the sensitive pad rows, the square cell of PC94 results in a relatively large charge sharing. To minimize this effect, in the PC95 prototype the cells were made wider and the relative width of the guard strips was increased (see Table 1). This prototype shows a charge sharing of the order of 2 to 3%, roughly half that of PC94. A further reduction of the charge sharing can be obtained by an additional increase of the guard strip width. However, this will lead to a smaller fraction of the charge being induced on the chevron pad and thus to a degrading of the position resolution.

The induced charge distributions were also calculated for each geometry using the CERN program GARFIELD [21]. The calculations include both the anode and field wires. The calculations reproduce the data fairly well. In particular, they reproduce the evolution of the charge sharing with the detector cell geometry. It should be noted that field wires have for effect of reducing the tail of the induced charge distribution and thus the amount of charge sharing. Calculations done using the empirical formula of Ref. [22] which considers only anode wires predict a charge sharing roughly 60% larger.

4. Conclusions

MWPC detectors with very long and narrow interpolating chevron cathode pads have been build. Such a geometry gives rise to very sharp angles. A truncated tip pattern has been developed which is more reproducible and gives a more reliable response than the standard chevron geometry. A position resolution of the order of 1%-1.5% of the readout spacing was achieved. A study of the dependence of the resolution on the amplitude of the signal shows that intrinsic resolution of the detector and the electronic noise contribute equally to the measured overall resolution. The detector response shows non-linearity which depends on the pad geometry. This non-linearity can, however, be easily corrected using simple analytical expression. The variation in the charge sharing between adjacent rows of pads, for the various geometries tested, was observed to be consistent with calculated values.

5. Acknowledgments

The authors wish to acknowledge the contribution of Richard Duguay, Sean McCorkle, Leo Nikkinen, and James Robar for their help in the prototype construction and during the beam test. This work is supported by the U.S. Department of Energy and the Natural Sciences and Engineering Research Council of Canada.

References

[1] The PHENIX collaboration, The PHENIX Conceptual Design Report, BNL-48922, (1993).

[2] J.Fisher, J. Fuhrmann, S. Iwata, R. Palmer, and V. Radeka, Nucl. Instr. Meth. 136 (1976) 19.

[3] C.J. Borkowski and M.K. Kopp, Rev. Sci. Instr. 46 (1975) 951.

[4] J.L. Alberi ad V. Radeka, IEEE Trans. Nucl. Sci. NS-23 (1976) 251.

[5] A.L.S. Angelis *et al.*, Nucl. Instr. Meth. Phys. Res. A283 (1989) 762.

[6] R. Debbe, j. Fisher, D. Lissauer, T. Ludlam, D. Makowiecki, V. Radeka, S. Reacia, G.C. Smith, D. Stephani, and B. Yu, Nucl. Instr. Meth. Phys. Res. A283 (1989) 772.

[7] G.C. Smith, J. Fisher, and V. Radeka, IEEE Trans. Nucl. Sci. NS-35 (1988) 409.

[8] E. Mathieson ad G.C. Smith, IEEE Trans. Nucl. Sci. NS-36 (1989) 305.

[9] O.H.W. Siegmund *et al.*, IEEE Trans. Nucl. Sci. S-30 (1983) 503.

[10] R. Allemand and G. Thomas, Nucl. Instr. Meth. 137 (1976) 141.

[11] D.F. Anderson, H.K. Arvela, A. Breskin, and G. Charpak, Nucl. Instr. Meth. 224 (1984) 315.

[12] J. Allison, R.J. Barlow, R.Canas, I.P. Duerdoth, F.K. Loebinger, A.A. Macbeth, P.G. Murphy, and K. Stephens, Nucl. Instr. Meth. A236 (1985) 284.

[13] T. Miki, R. Itoh, and T. Kamae, Nucl. Instr. Meth. A236 (1985) 64.

[14] R. Debbe *et al.*, IEEE Trans. Nucl. Sci. NS-37 (1990) 88-94.

[15] J. Fischer *et al.*, IEEE Trans. Nucl. Sci. NS-37 (1990) 82-87.

[16] B. Yu, G.C. Smith, V. Radeka, and E. Mathieson, IEEE Trans. Nucl. Sci. NS-38 (1991) 454.

[17] B. Yu, PhD Dissertation, Univ. of Pittsburg, 1991.

[18] G.C. Smith, B. Yu, J. Fisher, V. Radeka, and J.A. Harder, Nucl. Instr. Meth. Phys. Res. A323 (1992) 78.

[19] M. Benayoun *et al.*, Nucl. Instr. Meth. Phys. Res. A342 (1994) 483-494.

[20] M. Benayoun *et al.*, Nucl. Instr. Meth. Phys. Res. A345 (1994) 72-89.

[21] R. Veenhof, CERN Program Library entry W5050.

[22] E. Mathieson, Nucl. Instr. Meth. A270 (1988) 602.

Table 1
Cell geometry of the tested pad chambers.

	PC94	PC95		
		Sect. 1	Sect. 2	Sect. 3
$Anode - Cathode(mm)$	2.0	3.0	5.0	6.0
$Anode - Anode(mm)$	4.0	8.0	14.0	16.0
$Pad\ Length(mm)$	220.0	93.8	157.7	185.6
$Pad\ Width(mm)$	3.00	5.0	10.0	12.0
$Guard\ Strip\ Width(mm)$	0.50	2.60	3.40	3.40
$Trace\ Width(mm)$	0.25	0.20	0.30	0.30
f_x		1.22	1.12	1.10

Table 2
Position resolution measured in PC94 for the different patterns.

Chevron Pattern	"Normal" Tips			"Squared" Tips		
f_x	1.25	1.21	1.15	1.45	1.40	1.35
$\sigma_{x_{cor}-x_{true}}(mm)$	2.4	2.7	2.9	2.9	2.7	2.3

Table 3.
Percentage of charge induced on neighboring pad row.

	Beam Data (%)	^{55}Fe Data (%)	Calculation (%)
PC94	6.3		6.8
PC95-Sect. 1	2.6	2.0	2.7
PC95-Sect. 2	2.7	3.0	2.9
PC95-Sect. 3	2.9	3.8	3.8

Figure captions

Fig.1. Patterns of centered single chevron with: (a) "normal" tips; (b) "squared" tips; (c) squared tips and tails. Dashed lines indicate the anode wire and field wire position.

Fig.2. A cross section of the PC95 prototype.

Fig.3. Prototype chamber electronics chain.

Fig.4. Diagram of the setup for the prototype beam test.

Fig.5. Residual $x_{rec} - x_{true}$ for normal chevron pattern ($f_x = 1.25$). Here x_{rec} is reconstructed position, x_{true} is true position of the avalanche. The residual distributions and their dependence upon the avalanche location x_{true} are shown: (a,b) - without correction; (c,d)- with quadratic correction; (e,f) - with 'perfect' off-line correction.

Fig.6. Same as Fig.5 but for squared chevron with $f_x = 1.35$.

Fig.7. Comparison of the experimental $x_{rec} - x_{true}$ with the assumed linear (a) and quadratic (b) correction functions as a function of the avalanche location. (c,d) Corresponding residual distributions $x_{cor} - x_{true}$. These results are for squared chevron pattern with $f_x = 1.35$.

Fig.8. (a) Typical cathode charge distribution measured in PC94; (b) same for the second section of PC95; (c) Dependence of the position resolution on the total charge in PC94. Solid triangles correspond to the chevrons of normal type with $f_x = 1.25$ and open circles to squared type with $f_x = 1.35$; (d) Same as (c) for the three sections of PC95. The lines are fits to the data.

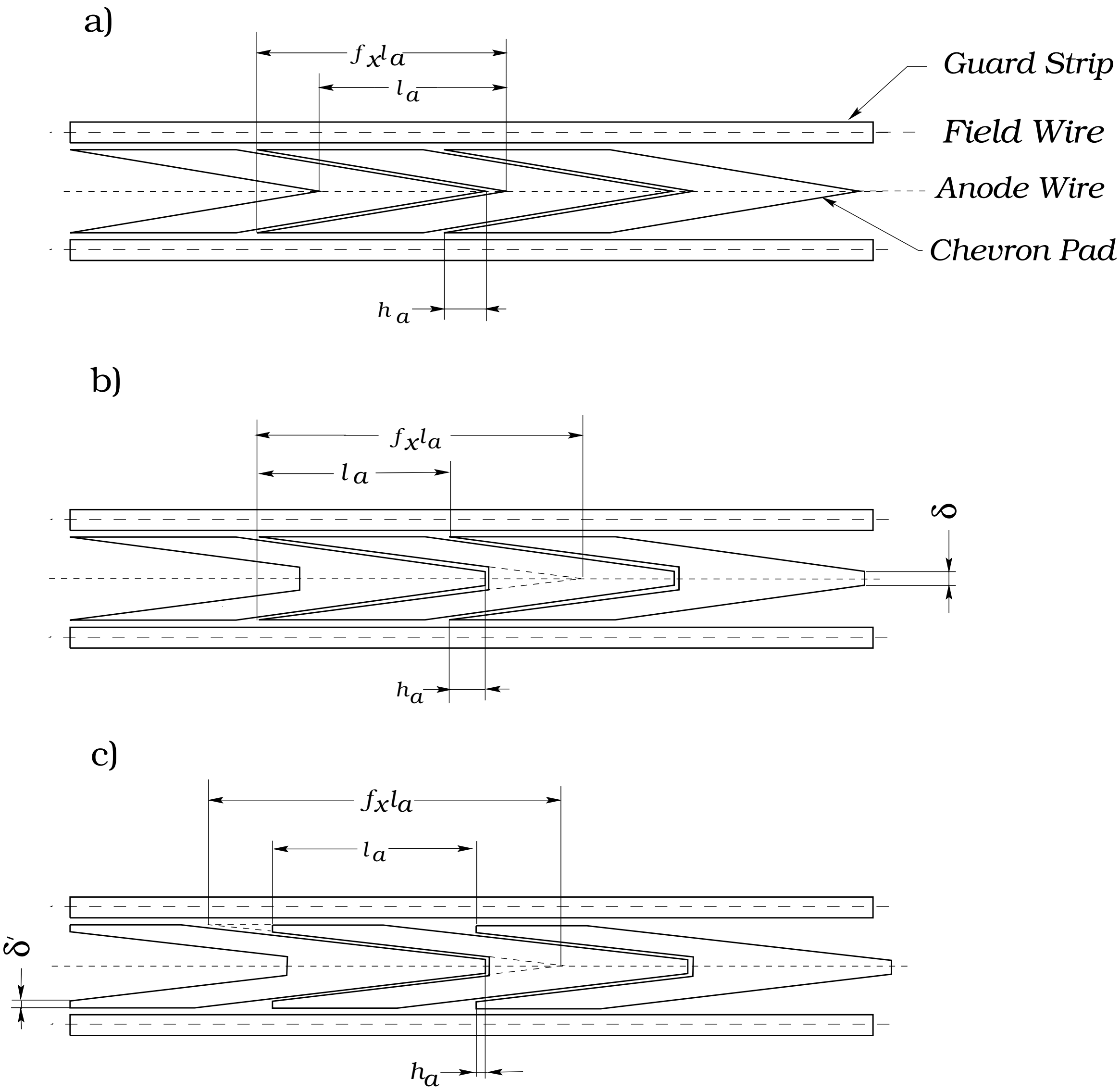
a)
$f_x l_a$
l_a
Guard Strip
Field Wire
Anode Wire
Chevron Pad
h_a
b)
$f_x l_a$
l_a
δ
h_a
c)
$f_x l_a$
l_a
δ
h_a

Figure 1:

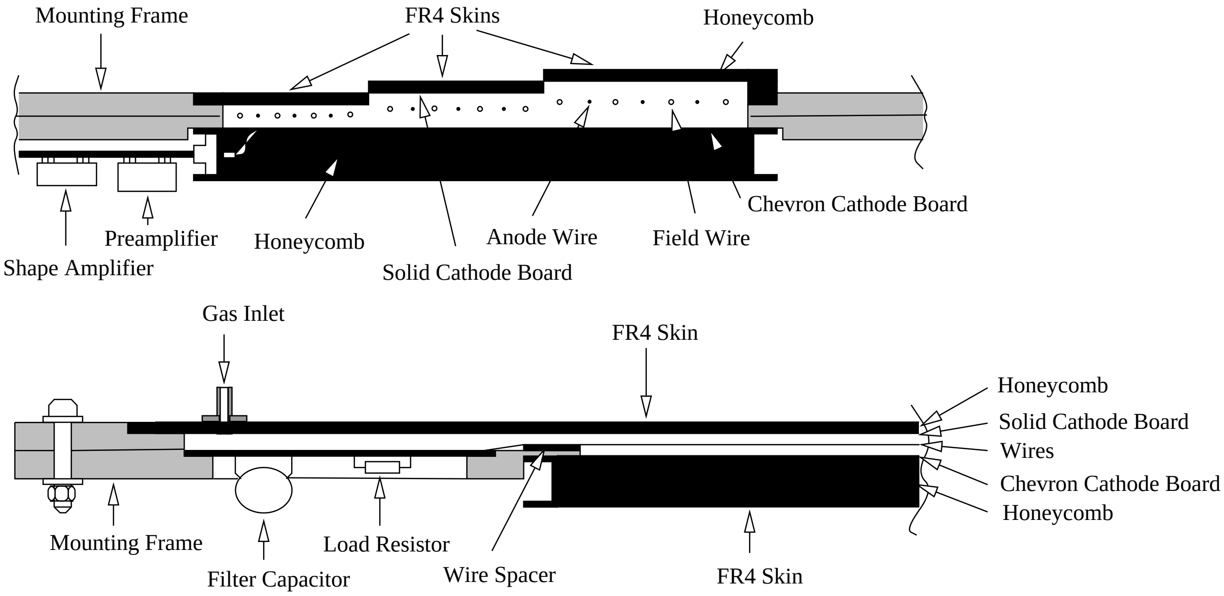
Mounting Frame
FR4 Skins
Honeycomb
Chevron Cathode Board
Shape Amplifier
Preamplifier
Honeycomb
Solid Cathode Board
Anode Wire
Field Wire
Gas Inlet
FR4 Skin
Honeycomb
Solid Cathode Board
Wires
Chevron Cathode Board
Honeycomb
Mounting Frame
Filter Capacitor
Load Resistor
Wire Spacer
FR4 Skin

Figure 2:

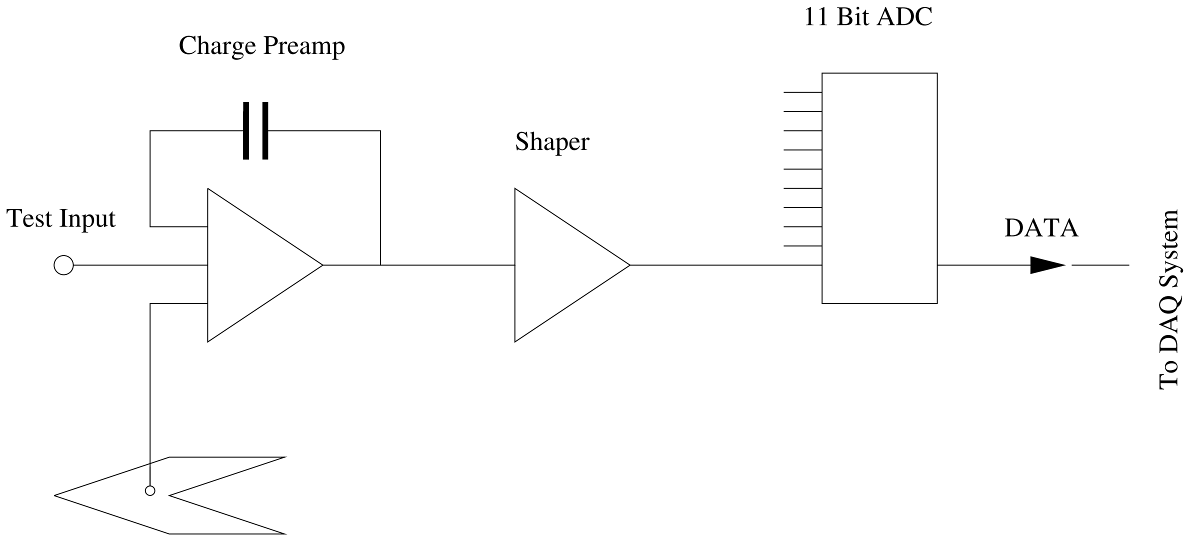
Charge Preamp
11 Bit ADC
Shaper
Test Input
DATA
To DAQ System

Figure 3:

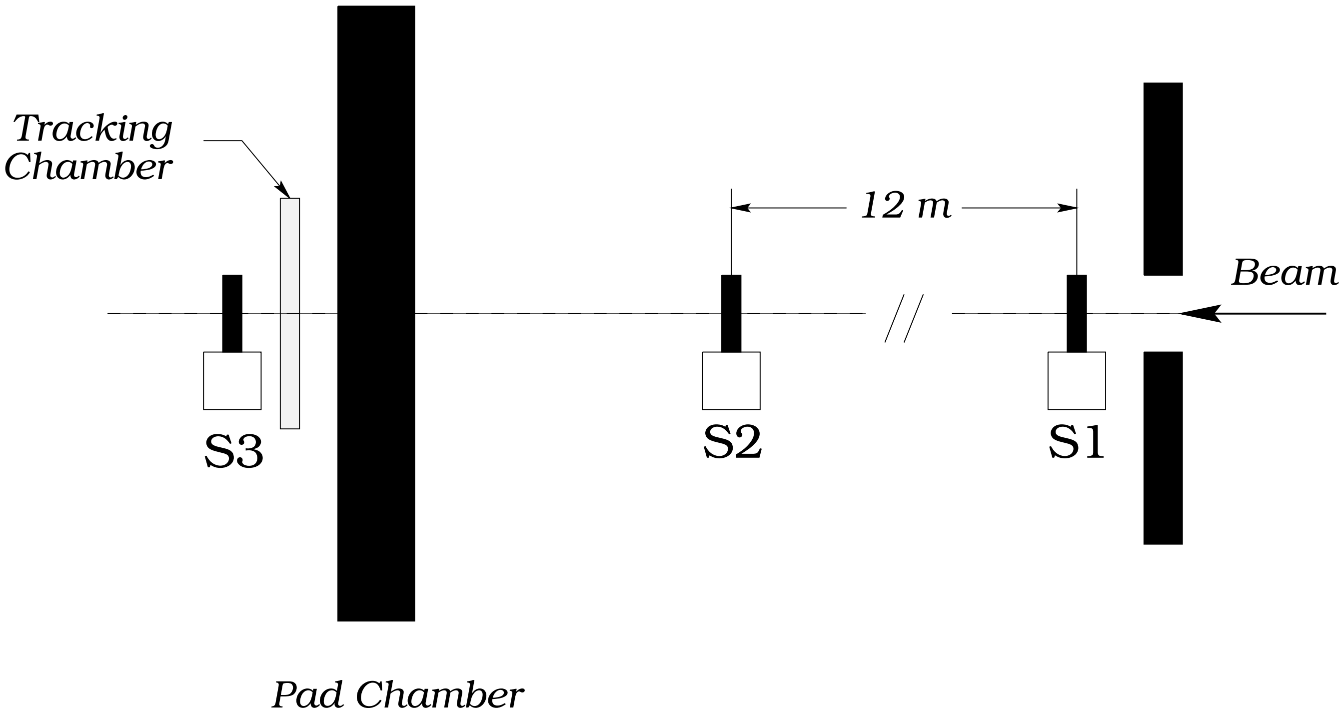

Figure 4:

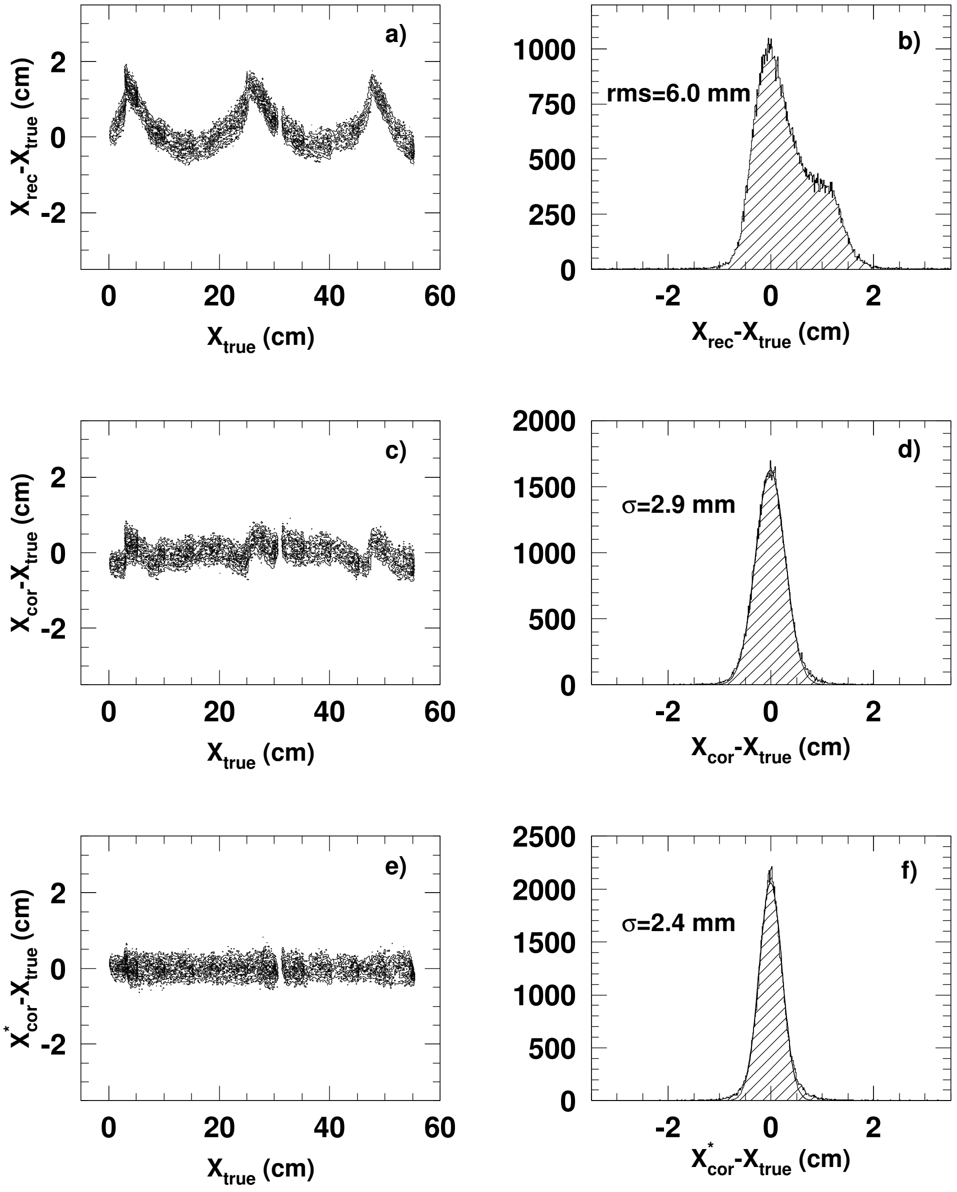
a)
b)
c)
d)
e)
f)
rms=6.0 mm
σ=2.9 mm
σ=2.4 mm
X_rec-X_true (cm)
X_cor-X_true (cm)
X*_cor-X_true (cm)
X_true (cm)

Figure 5:

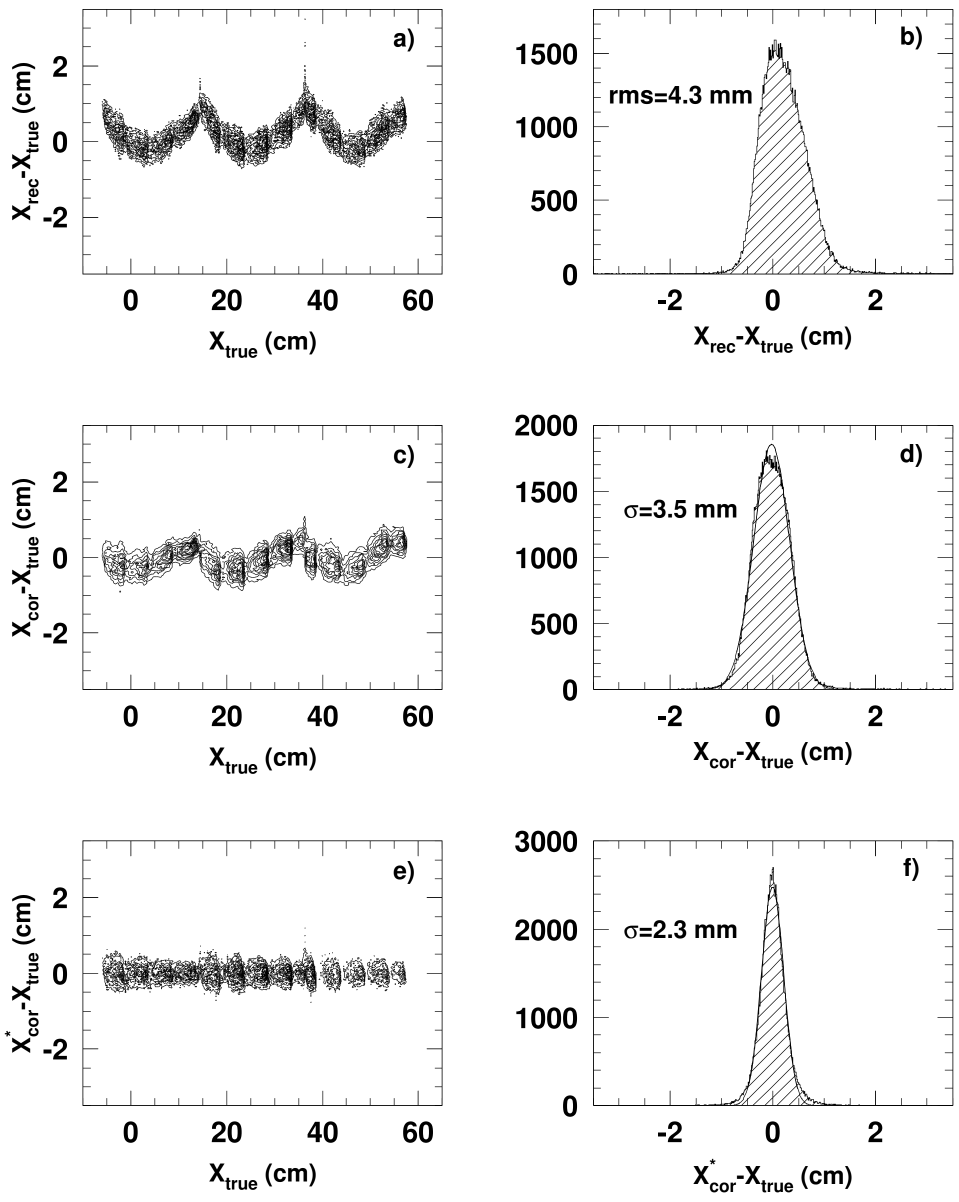
a)
b)
c)
d)
e)
f)
rms=4.3 mm
σ=3.5 mm
σ=2.3 mm
X_rec-X_true (cm)
X_cor-X_true (cm)
X*_cor-X_true (cm)
X_true (cm)

Figure 6:

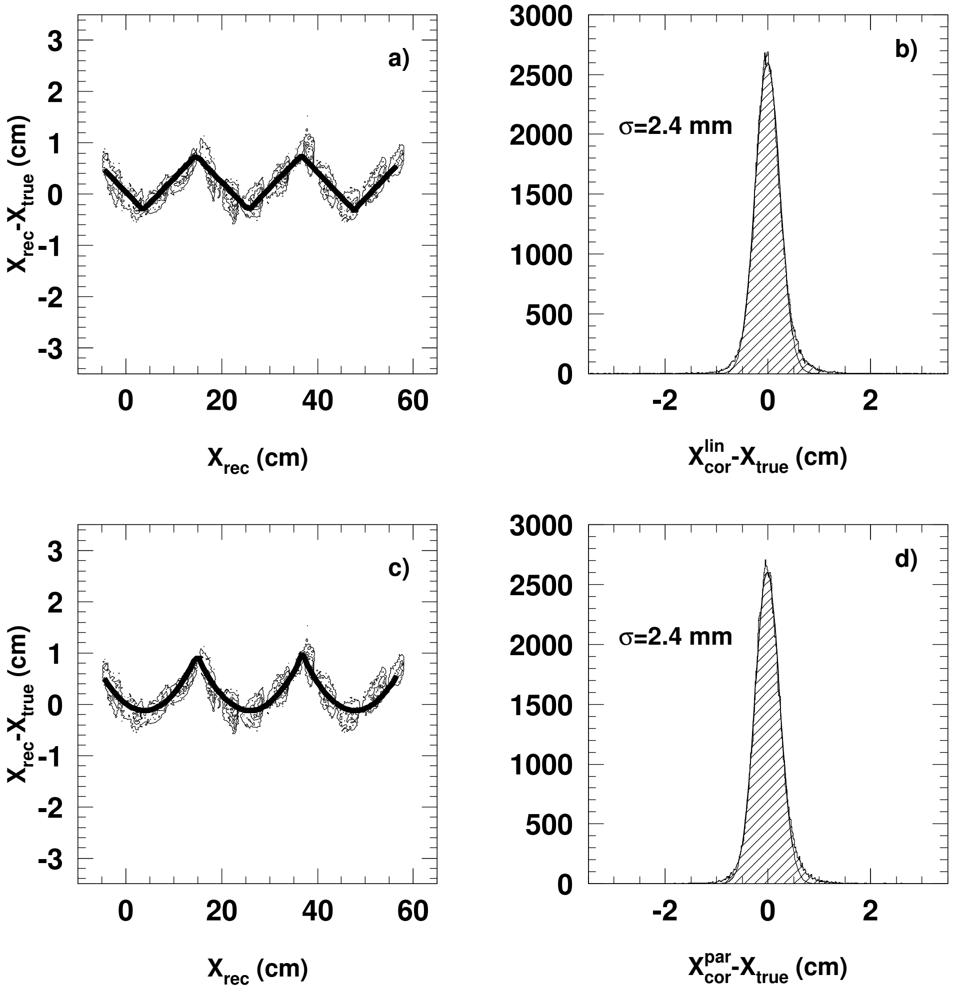
a)
b)
c)
d)
σ=2.4 mm
σ=2.4 mm
X_{rec}-X_{true} (cm)
X_{rec} (cm)
X^{lin}_{cor}-X_{true} (cm)
X_{rec}-X_{true} (cm)
X_{rec} (cm)
X^{par}_{cor}-X_{true} (cm)

Figure 7:

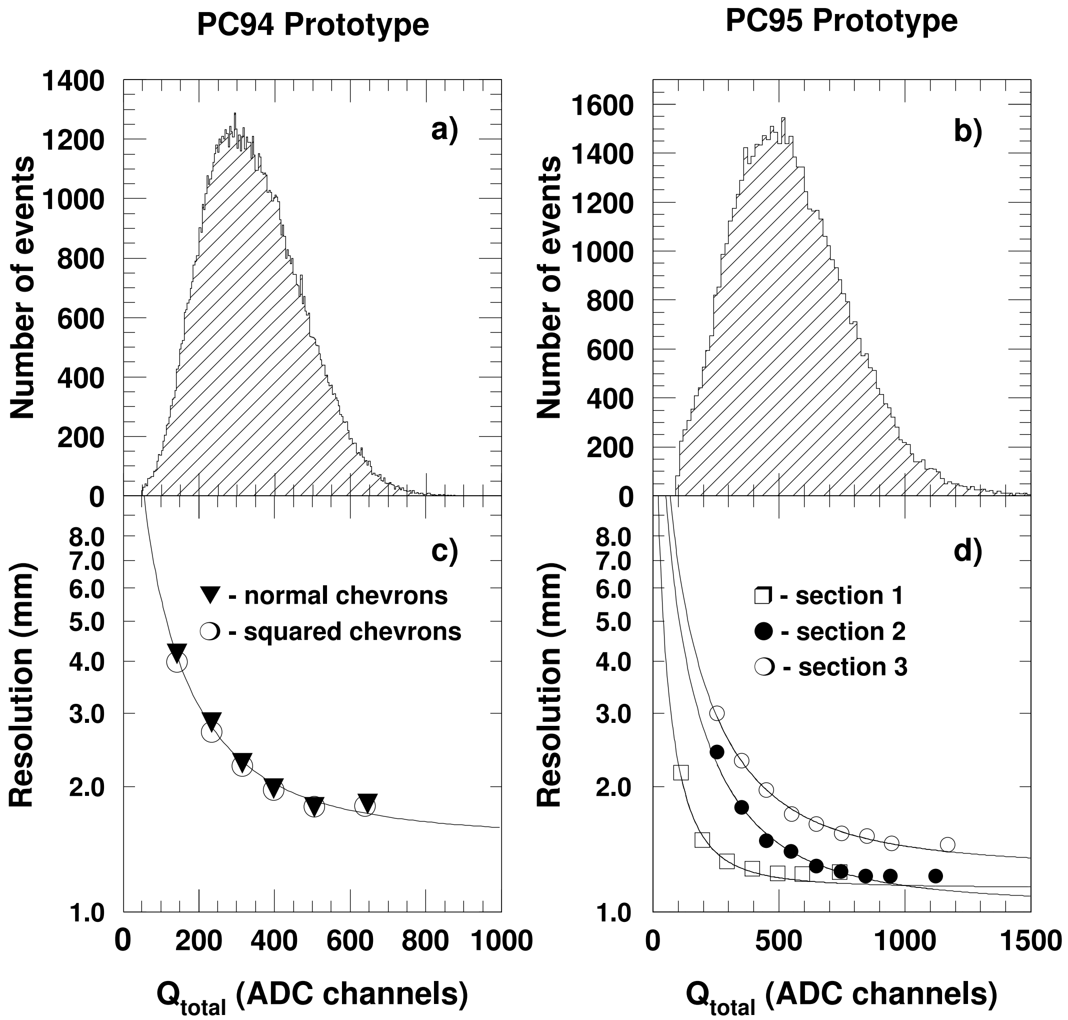

PC94 Prototype
PC95 Prototype
a)
b)
c)
d)
Number of events
Resolution (mm)
▼ - normal chevrons
❍ - squared chevrons
❐ - section 1
● - section 2
❍ - section 3
Q total (ADC channels)

Figure 8: